Scientific Research Publishing

Open Journal of Applied Sciences, 2026, 16(2), 487-498
https://www.scirp.org/journal/ojapps
ISSN Online: 2165-3925
ISSN Print: 2165-3917

Global Characterization of Solar Panels by Gabor Filters with a Texture Descriptor

Théodore Guié Toa Bi[1], Souleymane Tuo[1], Wognin Joseph Vangah[2], Charlotte Abalé[1], Sié Ouattara[3], Alain Clement[4]

[1]UFR Science and Technology, Département de Physique, University of Man, Man, Ivory Coast
[2]Unité de Recherche et d'expertise Numérique (UREN), Université Virtuelle de Côte d'Ivoire (UVCI), Abidjan, Côte d'Ivoire
[3]Institut National Polytechnique Houphouët Boigny (INPHB), Yamoussoukro, Côte d'Ivoire
[4]LARIS, SFR MATHSTIC, Université d'Angers, Angers, France
Email: theodore.toa@univ-man.edu.ci

How to cite this paper: Bi, T.G.T., Tuo, S., Vangah, W.J., Abalé, C., Ouattara, S. and Clement, A. (2026) Global Characterization of Solar Panels by Gabor Filters with a Texture Descriptor. *Open Journal of Applied Sciences*, **16**, 487-498.
https://doi.org/10.4236/ojapps.2026.162030

Received: June 6, 2025
Accepted: January 31, 2026
Published: February 3, 2026

Abstract

Accurate characterization of solar panel materials is essential to optimize their performance, durability, and recyclability. Conventional methods such as X-ray fluorescence, infrared spectroscopy, and X-ray energy-dispersive spectroscopy (EDS) can identify the chemical elements present, but remain costly, complex, and sometimes limited for detailed spatial analysis or access to certain structural information. This work proposes an alternative approach based on texture analysis by Gabor filter applied to images of photovoltaic modules. This method allows to quickly identify and distinguish the different components of solar panels. The study consisted of applying the Gabor filter to images of crystalline silicon panels in order to identify the main materials present and to evaluate their spatial distribution. The results show that the measured distances are below the threshold of 0.056, indicating a strong similarity between the analyzed powders and known references. The elements Si, Ag, Cu, CaO, Na_2O and SiO_2 were identified in the segmented regions, confirming the reliability of the textural approach for the analysis of photovoltaic materials. This method reduces analysis time and the need for specialized equipment, opening up prospects for better end-of-life management and optimization of photovoltaic panel recycling processes.

Keywords

Solar Panels, Characterization, Gabor Filter, Texture Analysis, Recycling, Photovoltaic Materials

1. Introduction

Characterizing the materials used in solar panel manufacturing is a crucial step in assessing their performance, durability, and recycling potential. For several years, physical and physicochemical methods such as X-ray fluorescence, infrared spectroscopy, and X-ray energy dispersive spectroscopy have been widely used for this purpose [1]. These techniques make it possible to identify the chemical constituents of photovoltaic cells, such as silicon, silver, copper, and molybdenum, with high accuracy. They are also used to analyze the composition of the glass covering the modules, identifying oxides such as SiO_2, Na_2O, CaO, and other elements present in the glass matrix [2]. However, despite their effectiveness, these methods have several limitations. They require expensive equipment, often involve complex preparation protocols, and require advanced technical skills, which limits their accessibility, especially in developing countries [3]. In addition, they are sometimes unable to detect internal irregularities or manufacturing defects in solar cells, especially when analyzing composite or old materials. Faced with these constraints, methods based on image analysis, and more specifically on texture analysis, appear as promising alternatives. Among them, the Gabor filter has distinguished itself by its ability to extract rich spatial and frequency information, by imitating the perception mechanisms of the human visual system [4]. This filter allows the analysis of structures at different scales and orientations, making it an ideal tool for the examination of complex surfaces such as those of powders from photovoltaic modules. In this context, our work proposes to use the Gabor filter, in association with a texture descriptor based on data from the main information components, to perform a global characterization of solar panels. This approach aims to overcome the limitations of conventional methods, while reducing costs, analysis times and technical requirements.

This work is structured in three stages. We will first present the methodology adopted, the tools used as well as the stages of image analysis integrating the minerals to be identified. The next stage is devoted to the presentation of the experimental results, followed by discussions on the contributions and limitations of the identification method implemented.

2. Materials and Methods

2.1. Materials

2.1.1. Technical Materials

For this study, we used a Solar Africa polycrystalline solar panel with the following electrical characteristics:

1) Maximum power (Pm): 35 W;
2) Maximum voltage (Vmp): 17.6 V;
3) Maximum current (Imp): 2 A;
4) Open-circuit voltage (Voc): 21 V;
5) Short-circuit current (Isc): 2.24 A.

This panel was recovered from the Ancienkan neighborhood, located in the

PALMCI village, near Divo, a city in the center-west of Côte d'Ivoire. Figure 1 below shows the polycrystalline solar panel studied in our study.

Figure 1. Photograph of the polycrystalline solar.

2.1.2. Experimental Device

Figure 2 shows the sieve used to sift the glass crystals and the VWR brand electronic balance shown in Figure 3 allowed us to make the different weighing of each quantity of powder of the panel components.

Figure 2. Sieve.

Figure 3. Electronic balance.

The glass crystal and filament samples were ground using a Retsch 200 mill (Figure 4) in manual mode, with a speed of 1100 rpm for 2 minutes and 40 seconds. These parameters were optimized to obtain a homogeneous powder while limiting mechanical heating and contamination, thus preserving the structural and chemical integrity of the materials.

Figure 4. Ritsch 200 Mill.

Image acquisition was performed using a smartphone equipped with a 26 mm wide-angle lens with an f/1.6 aperture. The 12-megapixel sensor with 1.4 μm pixels provides high-quality images, and autofocus enables sharp digital images.

MATLAB R2022a software, released on March 9, 2022, was used for data processing and visualization.

2.2. Methods

2.2.1. Solar Panel Disassembly

To disassemble the solar panel, a hammer was first used to gently break the glass into small fragments, facilitating its removal. The filaments were then manually extracted and cut into smaller sections using chisels for grinding [5].

2.2.2. Preparation of the PV Glass and Filament Powder

15 g of glass and filament were collected for powder processing. The glass and filament were ground separately using an electric grinder, reducing each material to fine, homogeneous particles. Before grinding, the resulting particles were sieved through a screen to separate the different particle sizes. **Figure 5** shows the glass and filament powders of the solar panel.

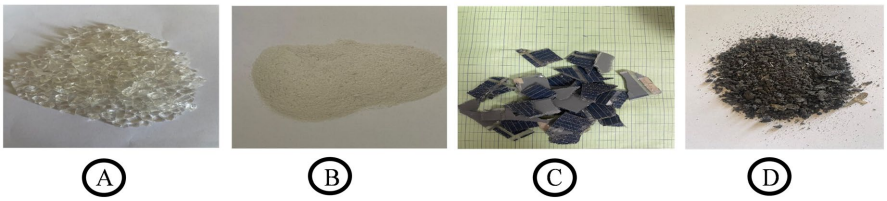

Figure 5. Glass crystals (A); Crushed glass powder (B); PV filament (C); Crushed filament powder (D).

2.2.3. Gabor Filter

In the analysis of the textures of glass and filament powders, the application of the Gabor filter made it possible to extract local characteristics related to frequency and orientation [6]. For this, we used a wavelength fixed at 4, which allows capturing fine details, as well as a maximum orientation of 90˚, corresponding to the

detection of vertically oriented patterns in the image [7]. This approach allowed us to obtain, for each material (glass and filament), two images resulting from the transformation: the magnitude image, which highlights the areas with a strong textural response, and the phase image, which provides information on the fine structure and organization of the patterns [8].

If we have an image $I(x,y)$ of dimension M × N pixels, its discrete Gabor wavelet transform is obtained by convolution with m orientations and n frequencies [9],

$$G_{m,n}(m,n)=\sum_{s}\sum_{t} I(x-s,y-t)\psi^{*}{}_{m,n}(s,t)$$

where $G_{mn}(x,y)$ is the Gabor wavelet transform, s, t are summation variables ψ^{*} is the conjugate of $\Psi(x,y)$ such that:

$$\Psi(x,y)=\frac{1}{2\pi\sigma_x\sigma_y}\exp\left[-\frac{1}{2}\left(\frac{x^2}{\sigma^2{}_x}+\frac{y^2}{\sigma_y{}^2}\right)+j2\pi.f\right]$$

Where $\Psi(x,y)$ represents the 2D Gabor function σ_x and σ_y are the standard deviations along the x and y axes, respectively f is the spatial frequency of the Gabor filter.

3. Results and Discussions

3.1. Analysis of Control and PV Powders

The analysis of the control powder table (Ag, Cu, Si, CaO, Na_2O, SiO_2) was performed using the Gabor filter applied to the obtained images (**Figure 6(A)** and **Figure 6(B)**). This approach made it possible to extract textural characteristics at two levels: magnitude, which provides information on the intensity of the detected structures, and phase, which highlights the orientation and continuity of the patterns. The use of these two components makes it possible to identify, for each material, a textural characteristic, useful for differentiating and identifying constituents in complex mixtures.

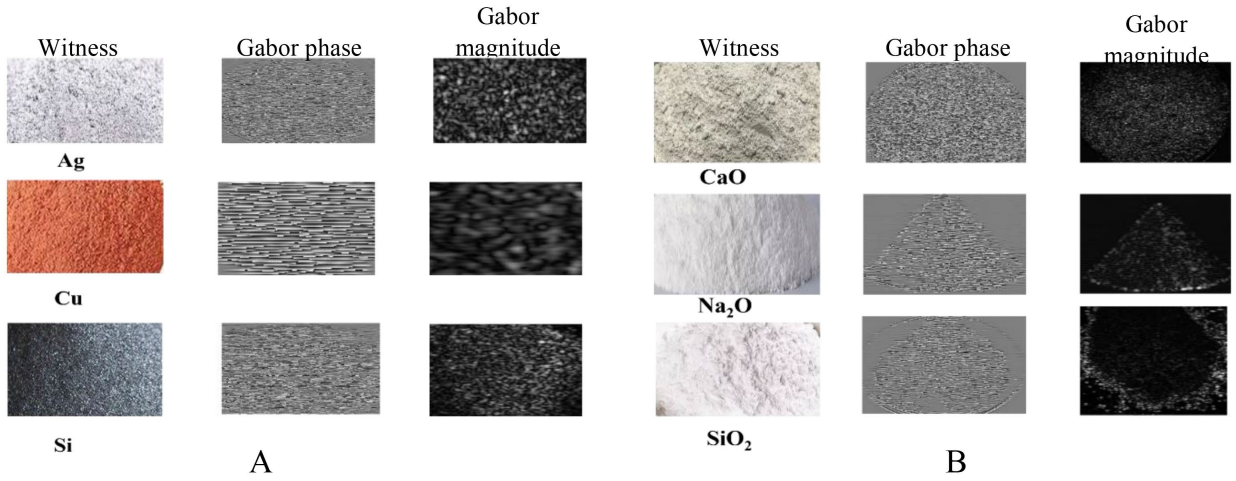

Figure 6. Filament witness powders (A); Glass witness powders (B).

3.2. Segmentation of the Different Powders

3.2.1. Segmentation of the Magnitudes of the Different Witness Powders and the PV

The segmentation was performed on the magnitude, considering areas with comparable textural intensity levels. For each segmented region, a set of parameters was extracted (at, bt, ct, dt, E, S) [11]. The results of this segmentation are presented in **Figure 7**.

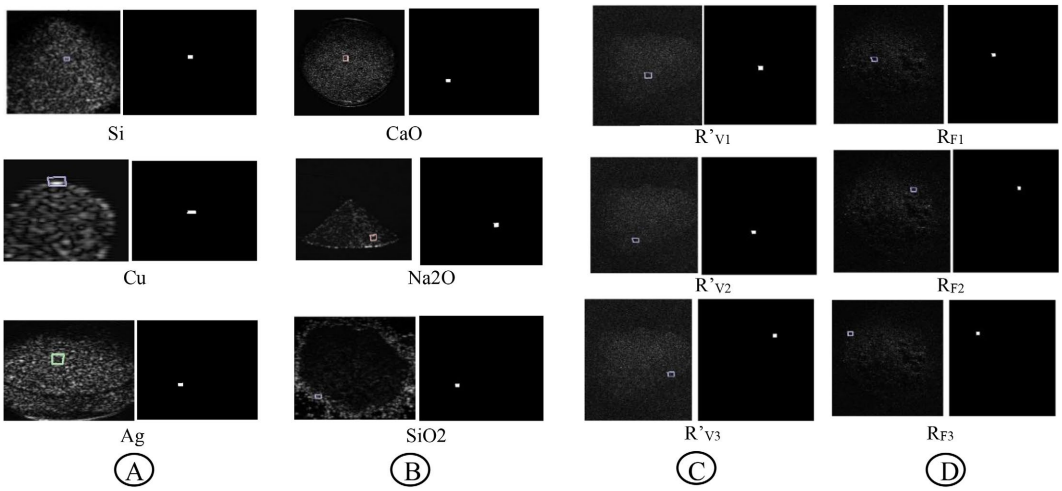

Figure 7. Segmentation of the magnitudes of the control powders (A) and (B); Segmentation of the magnitudes of the glass powders (C); Segmentation of the magnitudes of filament powders (D).

3.2.2. Segmentation of the Phases of the Different Witness Powders and the PV

Following the magnitude-based analysis, regional segmentation was also applied to the images from the Gabor filter phase, in order to better characterize the spatial and directional organization of the structures present in the control and photovoltaic powders [12]. **Figure 8** illustrates the segmentations performed on the control powders and the PV glass and filament powders.

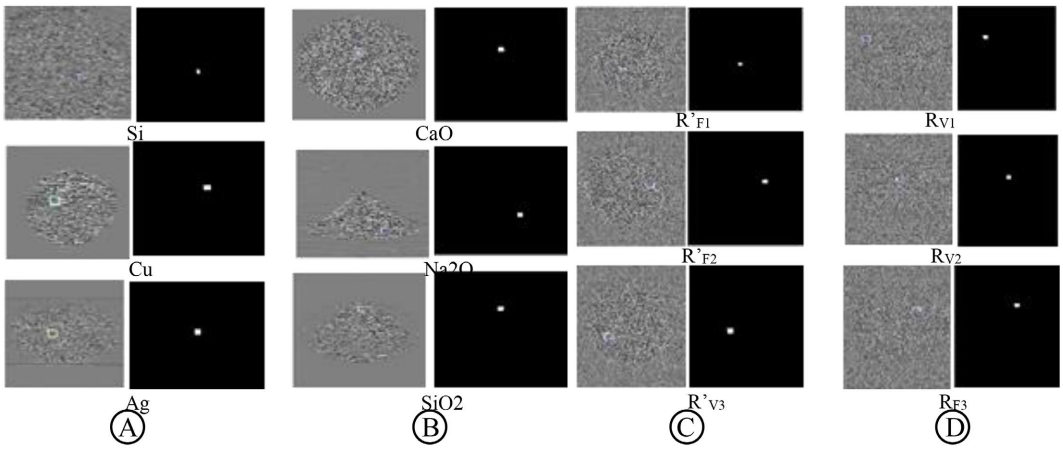

Figure 8. Phase segmentation of the filament (A) and glass (B) powders, Phase segmentation of the filament (C) and glass (D) powders.

3.3. Presentation of Characteristic Parameter Values after Segmentation

3.3.1. Characteristic Values Extracted from Magnitudes and Phases

Tables 1-3 and Table 4 group, respectively, the parameter values (at, bt, ct, dt, E, and S) of the magnitudes of the control glass and filament, the parameter values of the magnitudes of the PV glass and filament, the parameter values of the phases of the control glass and filament, and finally the parameter values of the phases of the PV glass and filament.

Table 1. Values of magnitude parameters.

Glass and Filament Mag (Witness))	CaO	Na_2O	SiO_2	Cu	Ag	Si
at	42.8746	48.4314	23.8113	24.9658	26.00	16.2771
bt	0.6318	0.3271	0.4494	0.5778	0.4614	0.7043
et	4.4554	23.1475	9.3894	88.9761	3.5475	8.3523
S	23.2127	20.0751	11.6776	17.4237	25.1772	14.8689
E	6.3757	6.0487	5.1364	5.7434	6.6637	5.4539
ct	356.038	289.393	468.9452	436.2436	285.0455	327.186

Table 2. Parameters of the magnitudes of the PV powders.

Glass and PV Filament Mag	R'_{V1}	R'_{V2}	R'_{V3}	R_{F1}	R_{F2}	R_{F3}
at	45.5589	42.415	23.6412	15.9527	24.7174	26.1691
bt	0.3162	0.6289	0.4002	0.7033	0.5665	0.4521
et	17.0889	5.8852	10.9592	7.6667	83.8205	3.662
S	26.7244	22.2599	12.5591	13.625	17.1222	21.6271
E	6.1268	6.2129	5.9053	5.3169	5.7	6.3432
ct	300.8554	359.6189	493.7983	327.856	437.4429	285.4401

Table 3. Phase parameter data of control samples.

Glass and filament phase (Witness)	CaO	Na_2O	SiO_2	Cu	Ag	Si
at	125.3464	128.2482	126.3348	132.5334	123.8497	128.3626
bt	0.4654	0.7166	0.6148	0.3941	0.7365	0.5367
et	9.6827	3.4451	4.9791	1.5581	3.5475	2.0684
S	54.2815	59.5657	58.2266	70.3802	69.4064	69.243
E	7.3235	7.5449	7.5302	7.6211	7.4495	7.8146
ct	345.5958	439.6475	206.9962	532.1771	452.1494	419.7774

Table 4. PV phase parameter data.

Glass phase and PV filament	R_{V1}	R_{V2}	R_{V3}	R'_{F1}	R'_{F2}	R'_{F3}
at	125.4261	126.4031	128.0255	128.021	122.4519	131.9045
bt	0.4421	0.6672	0.7711	0.5388	0.6749	0.3292
et	8.8553	3.3786	3.85	2.7872	3.5792	1.2211
S	52.7259	58.547	60.3977	69.2092	68.2759	70.3796
E	7.4592	7.5249	7.5305	7.7965	7.3566	7.5532
ct	331.9599	236.6931	402.81	416.6037	424.3883	529.4692

These different values made it possible to construct histograms in Figure 9 which give the distribution of parameter values according to the components (CaO, Na_2O, SiO_2, Cu, etc.) of the solar panel.

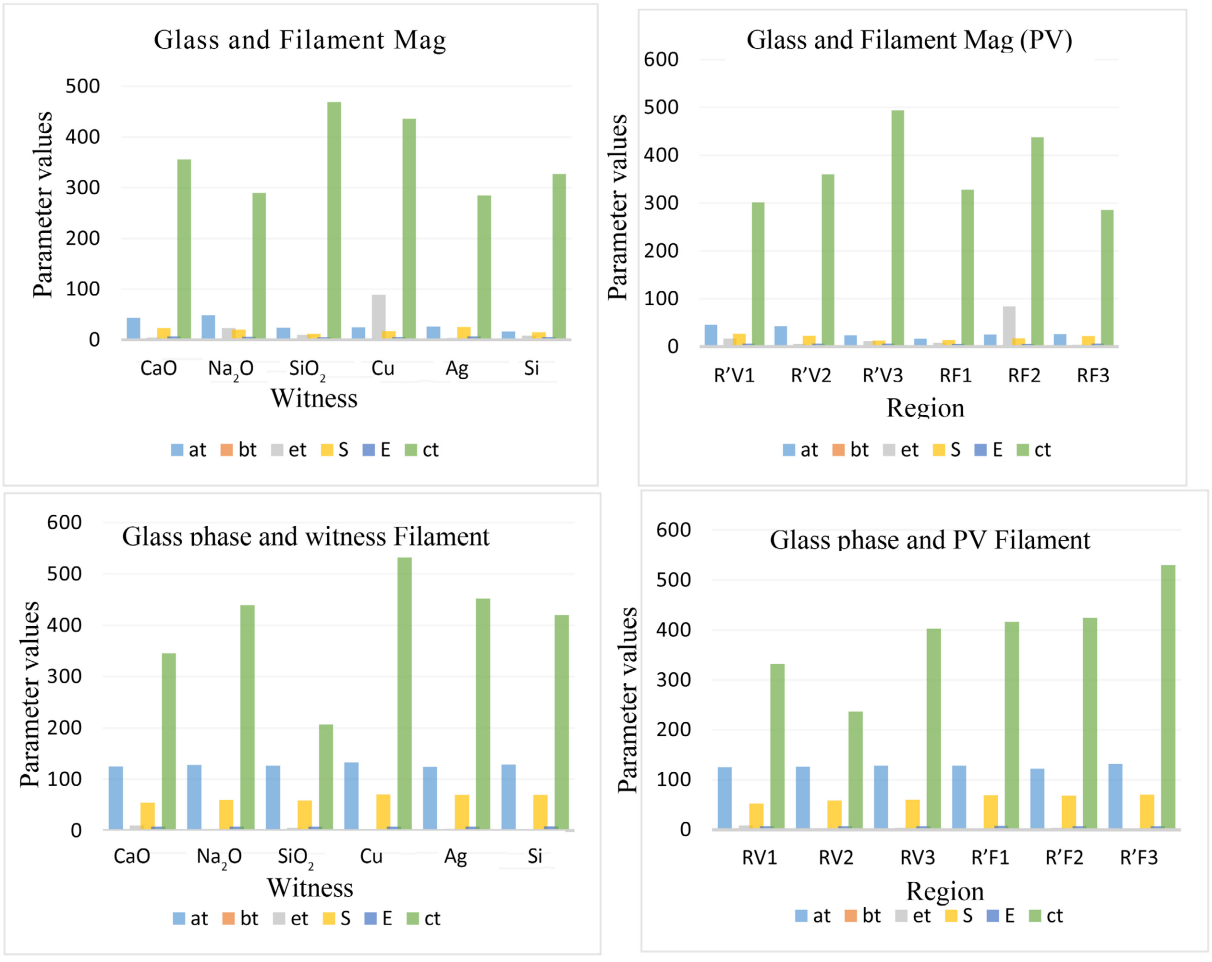

Figure 9. Magnitude and phase histograms of witnesses and PV (Filament and Glass).

The phase and magnitude histograms show, for each region analyzed (RV1, RV2, RV3, RF1, RF2, RF3), the distribution of textural parameters (at, bt, et, S, E, ct). By

comparing the profiles of the regions from the panel (glass and filament) with those of the controls, the chemical elements present in each region can be identified [13].

Analysis of the magnitude histograms confirms the trends observed with the phase. The R'V1, R'V2, and R'V3 regions respectively show a strong presence of Na_2O, CaO, and SiO_2, while the RF1, RF2, and RF3 zones are characterized by the dominant presence of Si, Cu, and Ag. Although the ct bar is predominant, the relative distribution of the other components (at, S, E, etc.) allows for the identification of the elements present in each region and the elimination of the presence of certain elements in the segmented region.

3.3.2. Ore Identification by Euclidean Distance

We used the normalized Euclidean distance to calculate the distance between the characteristic vectors of the components (ores). It is calculated using the following formula:

$$d_{norm}\left(R_i, T\right) = \sqrt{\frac{\sum\left(a_i - b_i\right)}{\sigma_i}}$$

Normalized Euclidean distance values were calculated to assess the magnitude variations between the control powders (glass and filament) and those from the photovoltaic panels. Table 5 and Table 6 present these distances, thus showing the similarity between the vectors of the different regions analyzed.

Table 5. Normalized Euclidean distances for the magnitude of control powders and PV powders.

Vectors	$(V_{R'V1};V_{Na2O})$	$(V_{R'V2};V_{CaO})$	$V_{R'V3};V_{SiO2})$	$(V_{F1};V_{Si})$	$(V_{F2};V_{Cu})$	$(V_{F3};V_{Ag})$
d_{norm}	0.0281	0.0209	0.0158	0.0032	0.0055	0.0047

Table 6. Normalized Euclidean distances for the phase of control powders and PV powders.

Vectors	$(V_{RV1};V_{CaO})$	$(V_{RV2};V_{SiO2})$	$V_{RV3};V_{Na2O})$	$(V_{F'1};V_{Si})$	$(V_{F'2};V_{Ag})$	$(V_{F'3};V_{Cu})$
d_{norm}	0.0086	0.0073	0.0124	0.0041	0.0068	0.0109

The distances are very small, ranging from 0.0032 to 0.0281 for magnitude, and from 0.0041 to 0.0124 for phase. These values are well below the threshold of 0.05 commonly used in the scientific literature to indicate a high similarity between two samples [14] [15]. This indicates that the powders from the photovoltaic panel have a chemical composition very close to that of the control powders. The magnitude analysis highlighted that some segmented regions of the image, such as R'V1, R'V2 and R'V3, are strongly correlated with the spectral signatures of Na_2O, CaO and SiO_2. Other regions, such as RF1, RF2 and RF3, show similarity with the reference powders containing Si, Cu and Ag. For the phase, the regions RV1, RV2 and RV3 also show very close profiles of CaO, SiO_2 and Na_2O. These results show that the Gabor filter, applied to powder images, not only allows textures to be differentiated, but also allows the chemical signatures characteristic of the elements present to be identified. A comparative analysis with classical chemical

methods, such as infrared spectroscopy and X-ray fluorescence, was carried out to validate these results. The studies of [16] and [17] all identified the same elements in polycrystalline photovoltaic panels as those detected in our study (Si, Ag, Cu, CaO, Na_2O, SiO_2). These comparisons reinforce the reliability of the results obtained with our image analysis method. Moreover, these results are consistent with those of [18] [19], who also used techniques based on texture analysis and Euclidean distances to identify chemical elements in materials. This methodological convergence shows that our approach is robust and can be used effectively in the characterization of photovoltaic materials. However, it is important to highlight some limitations of our method. Indeed, elements such as lead and tin, identified by [20] in photovoltaic panels using conventional chemical methods (EDS and atomic absorption spectroscopy), could not be detected in our study. This is explained by the fact that these elements were not part of the control powders selected for comparison, and that image segmentation does not always allow distinguishing all the components present in a complex sample.

4. Conclusion and Outlook

In this study, we were able to extract relevant parameters such as magnitude and phase from the Gabor parameters and filters, which proved essential for comparing the control powders with those from the panels. The small differences observed between the samples, with values systematically below the 0.05 threshold, indicated a strong similarity between the analyzed powders. These results show that the recovered powders contain components very similar to those of the reference powders, including elements such as Na_2O, CaO, SiO_2, Si, Cu, and Ag. This method makes it possible to accurately identify the different components of a powder when control powders are available for comparison. Furthermore, the results obtained are consistent with those of conventional analytical methods such as infrared (IR) spectroscopy and X-ray fluorescence (XRF), which reinforces the reliability of our approach. This study presents a very simple, rapid and less expensive alternative method for the identification of the components (recyclable minerals) of a polycrystalline solar panel.

Looking ahead, it will be interesting to expand the database of control powders by including elements not detected in this study (lead, tin, molybdenum, etc.) for a more in-depth characterization of the components of photovoltaic panels. We will also be able to couple Gabor filter analysis with advanced chemical techniques (EDS spectrometry, X-ray fluorescence, Raman spectroscopy) to validate and refine the results obtained.

Conflicts of Interest

The authors declare no conflicts of interest regarding the publication of this paper.

References

[1] Mousa, A., Al-Hamaiedeh, H. and Al-Kofahi, M. (2022) Elemental Analysis of Solar

Panels Using XRF and FTIR Spectroscopy. *Journal of Material Cycles and Waste Management*, **24**, 987-1001.

[2] Akel, S., Kulkarni, A., Rau, U. and Kirchartz, T. (2023) Relevance of Long Diffusion Lengthsfor Efficient Halide Perovskite Solar Cells. *PRX Energy*, **2**, Article ID: 013004. https://doi.org/10.1103/prxenergy.2.013004

[3] PV Magazine (2023) Organic Solar Panels: Advances and Applications. https://www.pv-magazine.com/organic-solar-panels

[4] Xu, Y., Quan, R., Xu, W., Huang, Y., Chen, X. and Liu, F. (2024) Advances in Medical Image Segmentation: A Comprehensive Review of Traditional, Deep Learning and Hybrid Approaches. *Bioengineering*, **11**, Article 1034. https://doi.org/10.3390/bioengineering11101034

[5] Choi, J.Y., Ro, Y.M. and Plataniotis, K.N. (2012) Color Local Texture Features for Color Face Recognition. *IEEE Transactions on Image Processing*, **21**, 1366-1380. https://doi.org/10.1109/TIP.2011.2168413

[6] Roy, S. and Maji, P. (2007) Texture-Based Classification Using Gabor Filters and Euclidean Distance Metrics. *IEEE Transactions on Image Processing*, **16**, 2128-2136.

[7] Wang, H.F., Zhang, K. and Ren, H.E. (2013) A Gabor Wavelet Transformation-Based Texture Images Classification Algorithm. *Advanced Materials Research*, **811**, 430-434. https://doi.org/10.4028/www.scientific.net/AMR.811.430

[8] Alferez, G.H., Vazquez, E.L., Martínez Ardila, A.M. and Clausen, B.L. (2021) Automatic Classification of Plutonic Rocks with Deep Learning. *Applied Computing and Geosciences*, **10**, Article ID: 100061. https://doi.org/10.1016/j.acags.2021.100061

[9] Chauhan, S., Rühaak, W., Anbergen, H., Kabdenov, A., Freise, M., Wille, T. and Sass, I. (2016) Phase Segmentation of X-Ray Computer Tomography Rock Images Using Machine Learning Techniques: An Accuracy and Performance Study. *Solid Earth*, **7**, 1125-1139. https://doi.org/10.5194/se-7-1125-2016

[10] Chen, X.L., Zhao, H.M., Li, P.X. and Yin, Z.Y. (2006) Remote Sensing Image Based on Analysis of the Relationship between Urban Heat Island and Land Use/Cover Changes. *Remote Sensing of Environment*, **104**, 133-146. https://doi.org/10.1016/j.rse.2005.11.016

[11] Bi, T.G.T., Ouattara, S. and Clément, A. (2018) Acquisition of Images by the Analysis of the Automatic Identification of Molecules in a Thin-Film Extract Combined with Laser. *Journal of Materials Physics and Chemistry*, **6**, 29-35.

[12] Lepistro, L., Kunttu, L. and Visa, A. (2005) Rock Image Classification Using Color Features in Gabor Space. *Journal of Electronic Image*, **14**, Article ID: 040503. https://doi.org/10.1117/1.2149872

[13] Vivek, C. and Audithan, S. (2014) Robust Analysis of the Rock Texture Image Based on the Boosting Classifier with Gabor Wavelet Features. *Journal of Theoretical and Applied Information Technology*, **69**, 562-570.

[14] Ishikawa, S.T. and Gulick, V.C. (2013) An Automated Mineral Classifier Using Raman Spectra. *Computers & Geosciences*, **54**, 259-268. https://doi.org/10.1016/j.cageo.2013.01.011

[15] Bi, T.G.T., Sandjé, M., Oscar, R.G., Ouattara, S. and Clement, A. (2022) A Semi-Vectorial Morphological Segmentation Multi-Component Images of Coumarins on Thin Layer Combined with Laser for Better Separation. *Open Journal of Applied Sciences*, **12**, 1054-1068. https://doi.org/10.4236/ojapps.2022.126072

[16] Yousuf, M.H., Saeed, F. and Tauqeer, H.A. (2022) Numerical Investigation of Cu_2O as a Hole Transport Layer for High-Efficiency, Cadmium Free CIGS Solar Cell.

https://doi.org/10.20944/preprints202110.0326.v2

[17] IEC 62446-3 (2020) Photovoltaic Systems—Testing, Documentation, and Maintenance Requirements. International Electrotechnical Commission.

[18] Bi, T.G.T., Vangah, W., Jérôme, A.N., Ouattara, S. and Clement, A. (2022) Image Acquisition and Parameter Calculations for Optimization of the Automatic Identification of Terpenes in a Combined Laser Thin Film Extract. *Advances in Materials Physics and Chemistry*, **12**, 141-154. https://doi.org/10.4236/ampc.2022.126010

[19] Mandadapu, U., Thyagarajan, K. and Vedanayakam, S.V. (2017) Simulation and Analysis of Lead Based Perovskite Solar Cell Using SCAPS-1D. *Indian Journal of Science and Technology*, **10**, 1-8. https://doi.org/10.17485/ijst/2017/v10i11/110721

[20] Camargo, P.S.S., Domingues, A.D.S., Palomero, J.P.G., Kasper, A.C., Dias, P.R. and Veit, H.M. (2021) Photovoltaic Module Recycling: Thermal Treatment to Degrade Polymers and Concentrate Valuable Metals. *Detritus*, **16**, 48-62. https://doi.org/10.31025/2611-4135/2021.15119